



# 1 Free Tropospheric Aerosols at the Mt. Bachelor Observatory: 2 More Oxidized and Higher Sulfate Content Compared to 3 Boundary Layer Aerosols

4 Shan Zhou<sup>1</sup>, Sonya Collier<sup>1</sup>, Daniel A. Jaffe<sup>2,3</sup>, Qi Zhang<sup>1\*</sup>

5 <sup>1</sup>Department of Environmental Toxicology, University of California, Davis, CA 95616, USA

6 <sup>2</sup>School of Science, Technology, Engineering, and Mathematics, University of Washington Bothell, Bothell, WA,  
7 USA

8 <sup>3</sup>Department of Atmospheric Sciences, University of Washington, Seattle, WA, USA

9 Correspondence to: Qi Zhang ([dkwzhang@ucdavis.edu](mailto:dkwzhang@ucdavis.edu))

## 10 Abstract

11 Understanding the properties and lifecycle processes of aerosol particles in regional air masses is crucial for  
12 constraining the climate impacts of aerosols on a global scale. In this study, characteristics of aerosols in the boundary  
13 layer (BL) and free troposphere (FT) of a remote continental region in the western US were studied using a high-  
14 resolution time-of-flight aerosol mass spectrometer deployed at the Mount Bachelor Observatory (MBO; 2763 m  
15 a.s.l.) in central Oregon in summer 2013. In the absence of wildfire influence, the average ( $\pm 1\sigma$ ) concentration of  
16 non-refractory submicrometer particulate matter (NR-PM<sub>1</sub>) at MBO was  $2.8 (\pm 2.8) \mu\text{g m}^{-3}$  and 84% of the mass was  
17 organic. The organic aerosol (OA) at MBO from these clean periods showed clear diurnal variations driven by the  
18 boundary layer dynamics with significantly higher concentrations occurring during daytime, upslope conditions. NR-  
19 PM<sub>1</sub> contained a higher mass fraction of sulfate and was frequently acidic when MBO resided in the FT. In addition,  
20 OA in the FT was found to be highly oxidized ( $O/C \sim 1.17$ ) with low volatility. In contrast, OA associated with BL  
21 air masses had an average  $O/C$  of 0.67 and appeared to be semivolatile. The significant compositional and physical  
22 differences observed between FT and BL aerosols may have important implications for understanding the climate  
23 effects of regional background aerosols.

## 24 1 Introduction

25 Atmospheric aerosols can scatter and absorb incident sunlight, therefore altering the radiation budget of the earth  
26 directly. Depending on their chemical composition and microphysical properties, aerosol particles can also act as  
27 cloud condensation nuclei and or ice nuclei and affect climate indirectly by altering the lifetime and optical properties  
28 of clouds. Understanding the properties and the lifecycle processes of atmospheric aerosols is important for reducing  
29 the uncertainties in aerosol climate forcing (Boucher, 2013).

30 Aerosols and their precursor gases are mostly emitted in the planetary boundary layer (PBL) but can be  
31 transported into the free troposphere (FT) through convection and frontal uplift. In the FT, aerosols are subjected to  
32 less efficient dry deposition and can have longer lifetimes than those in lower altitudes, facilitating regional



33 recirculation or long distance transport (Jaffe et al., 2005a; Dunlea et al., 2009; Sun et al., 2009). Under certain  
34 atmospheric conditions, aerosols in the FT can be entrained into the BL, affecting remote regions where local  
35 emissions may be minimal (Schroder et al., 2002; Timonen et al., 2013; Wang et al., 2016). A quantitative  
36 understanding of aerosol properties and processes in regional background air masses and in the FT is necessary for  
37 improving chemical transport models and global climate simulations.

38 High-altitude mountaintop observatories are important platforms for studying aerosols in regional air masses,  
39 especially in the FT without the added expense and difficulty of making airborne measurements. Various mountaintop  
40 sites have been operated in the US and Europe to perform long-term measurements on aerosol optical properties,  
41 number, and size distributions and trace gases in continental background air masses (Jaffe et al., 2005b; e.g., Van  
42 Dingenen et al., 2005; Reidmiller et al., 2010; Fischer et al., 2011; Hallar et al., 2011; Rose et al., 2015; Bianchi et al.,  
43 2016; Hallar et al., 2016; Tröstl et al., 2016; Zhang and Jaffe, 2017). Aerosol chemical composition has also been  
44 studied from high elevation sites, through both filter collection followed by offline analysis (e.g., Takahama et al.,  
45 2011; Hallar et al., 2013; Dzepina et al., 2015) and real-time measurements using online aerosol mass spectrometers  
46 (e.g., Zhang et al., 2007; Cozic et al., 2008; Sun et al., 2009; Fröhlich et al., 2015; Rinaldi et al., 2015; Freney et al.,  
47 2016). These measurements have provided valuable information on the chemical and physical properties of remote  
48 aerosols in the FT and PBL as well as how they are influenced by various sources (e.g., biomass burning, dust, and  
49 biogenic emissions) and atmospheric processes (e.g., new particle formation, long-range transport, and cloud  
50 processing).

51 The Mt. Bachelor Observatory (MBO) is a high-altitude atmospheric research site that has been utilized for  
52 studying atmospheric chemistry in the western U.S. (Weiss-Penzias et al., 2006; Timonen et al., 2013). The  
53 observatory is located at 2763 m above sea level at the summit of Mt. Bachelor, a dormant volcano in the Deschutes  
54 National Forest in central Oregon (43.98° N, 121.69° W). Due to its elevation, MBO is situated in the FT at night and  
55 is under the influence of upslope flow from the PBL air during the daytime (McClure et al., 2016). The remote  
56 characteristics of the site makes MBO an ideal location for studying transported plumes, such as biomass burning  
57 plumes from regional and distant sources (Jaffe et al., 2005b; Timonen et al., 2014; Briggs et al., 2016; Laing et al.,  
58 2016; Zhang and Jaffe, 2017; Zhang, 2018) and long-range transport of Asian pollution in the spring (Jaffe et al.,  
59 2005a; Weiss-Penzias et al., 2006; Fischer et al., 2010; Ambrose et al., 2011).

60 Continuous measurements of trace gases (e.g., ozone, carbon monoxide, carbon dioxide, mercury, nitrogen  
61 oxides) and aerosol optical properties have been made at MBO since 2004. In summer 2013, a high-resolution time-  
62 of-flight aerosol mass spectrometer (HR-AMS; Aerodyne Research, Inc.) was deployed at MBO as part of the US  
63 Department of Energy sponsored Biomass Burning Observation Project (BBOP) (Collier et al., 2016; Zhou et al.,  
64 2017). This was the first real-time, highly time-resolved aerosol chemical measurement study performed at this site.  
65 During this study, MBO was frequently impacted by transported wildfire plumes (Collier et al., 2016; Zhou et al.,  
66 2017) but there were two periods, July 25 – 30 and August 17 – 21, when the site was not influenced by wildfires and  
67 the concentrations of air pollutants remained low. Here, we focus on these clean periods to examine the chemical and  
68 physical properties of regional background aerosols and to investigate the differences of aerosol characteristics and  
69 processes in the PBL and the FT over Western US.

70 **2 Methods**

71 The HR-AMS was deployed at MBO from July 25 to August 25, 2013, as part of the BBOP campaign. Ambient  
72 aerosols were drawn through a PM<sub>2.5</sub> cyclone inlet and dehumidified by a Nafion dryer to eliminate potential RH  
73 effects on collection efficiency (CE). Treated particles then alternated between a heated thermodenuder (TD) line and  
74 an ambient bypass line every 5 minutes before entering the HR-AMS. Aerosol scattering (TSI nephelometer; 1 μm  
75 size cut), aerosol absorption (Tricolor Absorption Photometer, Brechtel; 1 μm size cut), CO and CO<sub>2</sub> (Picarro Cavity  
76 Ring-Down Spectroscopy G2502), O<sub>3</sub> (Dasibi), NO<sub>x</sub> (Air Quality Design 2-channel chemiluminescence), NO<sub>y</sub>  
77 (chemiluminescence), and peroxyacetyl nitrate (PAN; custom gas chromatograph) were also measured. Water vapor  
78 mixing ratios were calculated from the measured temperature, relative humidity (Campbell Scientific HMP 45C) and  
79 pressure (Vaisala PTB101B) following Bolton (1980), and typically agreed to within ± 15% and ± 0.3 g kg<sup>-1</sup> (Ambrose  
80 et al., 2011). Additional details of the instrumentation and methodology can be found in previous publications (Briggs  
81 et al., 2016; Collier et al., 2016; Zhou et al., 2017).

82 HR-AMS data were analyzed using established data analysis software tool Squirrel (v1.53) and Pika (v1.12;  
83 <http://cires1.colorado.edu/jimenez-group/ToFAMSResources/ToFSoftware>). A composition-dependent CE was  
84 applied based on the algorithm by Middlebrook et al. (2012) to account for possible CE changes induced by changes  
85 in particle phase in the AMS. A time-dependent gas phase CO<sub>2</sub><sup>+</sup> subtraction (Collier and Zhang, 2013) was performed  
86 to improve the quantification of organic aerosol (OA), which is critical for low aerosol loading conditions (Setyan et  
87 al., 2012). Elemental analysis of high-resolution mass spectra (HRMS) utilized both the Aiken-Ambient (AA) method  
88 (Aiken et al., 2008) and the Improved-Ambient (IA) method (Canagaratna et al., 2015).

89 Positive Matrix Factorization (PMF) was executed using the PMF2 algorithm (Paatero and Tapper, 1994) in the  
90 PET v2.05 program (Ulbrich et al., 2009) on the combined spectral matrices of organic and inorganic species (Sun et  
91 al., 2012; Zhou et al., 2017) during the clean periods without wildfire impact (i.e., July 25 – 30 and August 17 – 21).  
92 Organic ions at *m/z* 12 – 180 and major inorganic ions, i.e., SO<sup>+</sup>, SO<sub>2</sub><sup>+</sup>, HSO<sub>2</sub><sup>+</sup>, SO<sub>3</sub><sup>+</sup>, HSO<sub>3</sub><sup>+</sup>, and H<sub>2</sub>SO<sub>4</sub><sup>+</sup> for sulfate,  
93 NO<sup>+</sup> and NO<sub>2</sub><sup>+</sup> for nitrate, NH<sup>+</sup>, NH<sub>2</sub><sup>+</sup>, and NH<sub>3</sub><sup>+</sup> for ammonium, and HCl<sup>+</sup> for chloride were included. The error matrix  
94 was pre-treated based on the procedures described in Ulbrich et al. (2009). After PMF analysis, the mass concentration  
95 of each OA factor was derived from the sum of organic signals in the corresponding mass spectrum after applying the  
96 default relative ionization efficiency (RIE = 1.4) for organics and the time-dependent CE. The solutions for 2 to 5  
97 factors were explored with varying rotational parameters (-0.5 ≤ FPEAK ≤ 0.5, in increments of 0.1). Following the  
98 procedure listed in Table 1 in Zhang et al. (2011), PMF solutions were evaluated by investigating the key diagnostic  
99 plots, mass spectra, correlations with external tracers, and diurnal profiles. As shown in Fig. S1 in the supplementary  
100 material, the 2-factor solution showed relatively large residual while the 4-factor solution showed signs of factor  
101 splitting. The 3-factor solution resolved a less oxidized oxygenated OA (OOA) factor, a more oxidized OOA  
102 associated with some sulfate signals, and a sulfate-dominated OOA (Figs. S2 and S3). As the sulfate-dominated OOA  
103 accounted for only 3% of the total organic signal and its O/C and HRMS highly resembled those in the more-oxidized  
104 OOA factor (Fig. S3), these two factors were combined to form a so-called “highly oxidized OOA” factor which has  
105 an O/C of 1.17. Based on the chemical, physical characteristics and the volatility properties (see detailed discussions  
106 in Sect. 3.3), the less oxidized OOA was found to be semi-volatile OOA (SV-OOA) mainly associated with fresher



107 air masses from the BL whereas the highly oxidized OOA was comprised of low-volatility organic compounds (LV-  
108 OOA) representing regional background OA in the FT. Furthermore, the time series and mass spectra of the SV-OOA  
109 and LV-OOA derived here agreed well with the two background OOAs derived from PMF analysis of the whole  
110 dataset, including periods influenced by wildfires (Zhou et al., 2017) (Figs. S4 and S5;  $r^2 > 0.9$ ). All aerosol data in  
111 this analysis are reported at ambient condition, except for aerosol light scattering, which is reported at STP ( $T = 273\text{K}$   
112 and  $P = 1013.25\text{ hPa}$ ).

### 113 3 Results and Discussion

#### 114 3.1. Temporal and Diurnal Variations of Regional Background Aerosols Observed at MBO

115 While observations at MBO were made continuously from July 25 to August 25, for this work, we use only data  
116 from July 25 to 30 and August 17 to 21, 2013, which were relatively clear periods, free of wildfire influence. As  
117 shown in Fig. 1, throughout the clear periods, the CO mixing ratio and submicron aerosol light scattering at 550 nm  
118 ( $\sigma_{550\text{nm}}$ ) were below 120 ppb and  $25\text{ Mm}^{-1}$  at STP, respectively, similar to values previously observed at MBO under  
119 clean conditions (Fischer et al., 2011; Timonen et al., 2014). The site was influenced by transported wildfire plumes  
120 during the other periods of BBOP and air pollutant levels increased substantially, e.g., CO and  $\sigma_{550\text{nm}}$  increased by up  
121 to 8–10 times compared to the clean periods and NR- $\text{PM}_{10}$  reached up to  $140\text{ }\mu\text{g m}^{-3}$  (Zhou et al., 2017). During the  
122 clean periods, the HR-AMS indicator for biomass burning influence, namely the fraction of  $\text{C}_2\text{H}_4\text{O}_2^+$  ( $m/z = 60.021$ )  
123 signal over total OA ( $f_{60}$ ), was below 0.3% (Fig. S6), confirming negligible influence from BB (Cubison et al., 2011).  
124 Aerosol absorption data were available for the second clean period (August 17–21) and the average ( $\pm 1\sigma$ ) EC mass  
125 concentrations were estimated to be only  $0.04 (\pm 0.14)\text{ }\mu\text{gC m}^{-3}$ , further indicating a lack of BB influences.  
126 Additionally, although winds at MBO showed a persistent westerly component (Fig. 1a and Fig. S7b), the bivariate  
127 polar plot of NR- $\text{PM}_{10}$  concentrations exhibited a dispersed profile (Fig. S7c), indicating regional sources of aerosols  
128 during the clean periods.

129 The average ( $\pm 1\sigma$ ) concentration of NR- $\text{PM}_{10}$  (= sulfate + ammonium + nitrate + organics + chloride) during  
130 these two clean periods was  $2.8 (\pm 2.8)\text{ }\mu\text{g m}^{-3}$ . OA was the largest  $\text{PM}_{10}$  component, contributing on average  $\sim 84\%$   
131 to the total NR- $\text{PM}_{10}$  mass, followed by sulfate (11%), ammonium (2.8%), nitrate (0.9%), and chloride (0.1%) (Fig.  
132 S7a). Aerosol concentration and composition varied noticeably and showed diurnal changes that appeared to be mainly  
133 driven by BL dynamics. This is because MBO sits in the FT at night but is influenced by air masses transported from  
134 the PBL as the mixed layer height grows during the day. Indeed, the diurnal profile of the mixing-layer height retrieved  
135 from the HYbrid Single Particle Lagrangian Integrated Trajectory (HYSPLIT) model (Draxler, 1998) shows that the  
136 MBO is within the PBL between 12–8 pm PST (Fig. 2). In addition, previous studies at MBO have shown that water  
137 vapor mixing ratio ( $\text{H}_2\text{O}_{(\text{g})}$ ) can be used to differentiate BL-influenced and FT air masses as FT conditions tend to be  
138 very dry (Weiss-Penzias et al., 2006; Reidmiller et al., 2010; McClure et al., 2016; Zhang and Jaffe, 2017).  $\text{H}_2\text{O}_{(\text{g})}$  at  
139 MBO varied from as low as  $0.42\text{ g kg}^{-1}$  at night to as high as  $6.9\text{ g kg}^{-1}$  during the day (Fig. 1b) and showed a strong  
140 diurnal cycle similar to BLH and  $\text{NO}_y/\text{CO}$  (Fig. 2), another parameter for differentiating BL-influenced and FT air  
141 (Stohl et al., 2002).



142 NR-PM<sub>1</sub> and  $\sigma_{550\text{nm}}$  generally followed the temporal trend of H<sub>2</sub>O<sub>(g)</sub> (Fig. 1b and c) and presented a pronounced  
143 diurnal profile with substantial daytime enhancements (Fig. 2). The median mass concentration of NR-PM<sub>1</sub> was 0.5  
144  $\mu\text{g m}^{-3}$  at night and increased by more than 10 times to 5.6  $\mu\text{g m}^{-3}$  in the afternoon. Similar temporal variations and  
145 substantial daytime increases were observed for OA, nitrate, and gaseous pollutants such as CO, NO<sub>y</sub>, and  
146 peroxyacetyl nitrate (PAN) (Figs. 1 and 2), indicating that these species are primarily emitted or formed within the  
147 BL and their concentrations at MBO are strongly influenced by BL dynamics. At night, the site is situated in the FT,  
148 above the shallow nocturnal BL formed over the surrounding lower areas and disconnected from aerosol and gas  
149 sources at the low altitudes. As the BL grows during the day, convective transport and thermal winds entrain pollution  
150 from lower altitudes and increase air pollutants at the site. In contrast, sulfate and ammonium exhibited relatively  
151 constant concentrations (Fig. 1e) and less pronounced diurnal patterns (Fig. 2). The weaker influence from BL  
152 evolution indicates similar sulfate and ammonium concentrations in the BL and in the FT in the remote continental  
153 region of the western US and is consistent with the relatively long atmospheric lifetime and the regional characteristics  
154 of sulfate particles. O<sub>3</sub> and NO<sub>2</sub> mixing ratios also showed flat diurnal patterns (Fig. 2). However, a previous study at  
155 MBO indicates that O<sub>3</sub> is typically higher in FT air masses (Zhang and Jaffe, 2017) but this depends on the air mass  
156 origin and photochemical processing in both the BL and FT.

157 NR-PM<sub>1</sub> composition varied diurnally with a predominant organic composition during the day (up to 94% of  
158 NR-PM<sub>1</sub> mass; Figs. 1 and 2). However, at night when the site was situated in the FT, sulfate was a major component  
159 of aerosol (max = 83% of NR-PM<sub>1</sub>; median = 37.6%; mean = 33%). OA during the clean periods at MBO was oxidized  
160 with an average ( $\pm 1\sigma$ ) O/C of 0.85 ( $\pm 0.36$ ) and OM/OC of 2.26 ( $\pm 0.46$ ). The degree of oxidation was in agreement  
161 with regional background OA observed at other mountain sites such as Whistler Mountain in western Canada (Sun et  
162 al., 2009), Rocky Mountains in Colorado US (Schurman et al., 2015), and Mt. Cimone in Italy (Rinaldi et al., 2015).  
163 In addition, OA observed under the FT condition was overall more oxidized than those in the BL-influenced air  
164 masses. For example, O/C peaked at night with a maximum value of 1.5 and reached a minimum of 0.7 in the afternoon  
165 (Fig. 2). H/C anti-correlated with O/C with a reversed diurnal trend that peaked during daytime. As a result, the average  
166 oxidation state of carbon (OS<sub>C</sub>; = 2 O/C – H/C; (Kroll et al., 2011)) of OA at MBO during clean periods differs by 2  
167 units between day and night (Fig. 2). These trends highlight the different chemical properties as well as atmospheric  
168 ages of aerosols in the BL and the FT in this remote continental region in the western US. More discussions on the  
169 differences between aerosols in BL and FT air masses are given in Section 3.4.

### 170 3.2. Organonitrates and Organosulfates in Regional Background Aerosols

171 Particulate organonitrates have been shown to make a significant contribution to submicron aerosol mass,  
172 especially in rural and remote environments during summertime (Setyan et al., 2012; Fry et al., 2013; Kiendler-Scharr  
173 et al., 2016; Zhou et al., 2016). In this study, organonitrates were observed and appeared to account for most of the  
174 NO<sup>+</sup> and NO<sub>2</sub><sup>+</sup> (major ions of inorganic and organic nitrates in HR-AMS) signals detected in NR-PM<sub>1</sub> during the clean  
175 periods. This is because the signal ratios of NO<sup>+</sup> and NO<sub>2</sub><sup>+</sup> measured for MBO aerosols, which ranged between 2.0  
176 and 34.4 (average = 7.5; Fig. S9a), are substantially higher compared to the ratio for pure ammonium nitrate particles  
177 ( $R_{\text{AN}} = 1.78 \pm 0.07$ ). Previous studies reported that the NO<sup>+</sup>/NO<sub>2</sub><sup>+</sup> ratio for organonitrates ( $R_{\text{ON}}$ ) are ~2.25 - 3.7 times



178 higher than  $R_{AN}$  (Fry et al., 2009; Farmer et al., 2010; Fry et al., 2013). Based on this information and using the  
179 equation (1) reported in Farmer et al. (2010), we estimated that nearly all the  $NO^+$  and  $NO_2^+$  signals measured during  
180 the clean periods were contributed by organonitrates ( $RONO_2$ ) from the fragmentation of the nitrate functional group  
181 ( $-ONO_2$ ). Assuming that organonitrate molecules on average contain one  $-ONO_2$  functional group per molecule and  
182 have an average molecular weight of  $230 \text{ g mol}^{-1}$  (Lee et al., 2006; Fry et al., 2009), we estimated that the average  
183 concentration of organonitrates was  $0.13 (\pm 0.12) \mu\text{g m}^{-3}$  (Fig. S9b) and accounted for  $\sim 5\%$  of the total OA mass at  
184 MBO during the clean periods. Since MBO is situated in a forested region covered by coniferous trees at lower  
185 elevations, the reactions of monoterpenes with nitrate radicals were likely an important source of the observed  
186 particulate organonitrates (Fry et al., 2009; Fry et al., 2013; Boyd et al., 2015; Ng et al., 2017) in upslope daytime air.

187 The presence of organosulfur compounds is also confirmed based on the unambiguous detection of sulfur-  
188 containing organic ions ( $C_xH_yS_qO_z^+$ ) such as  $CH_2SO_2^+$ ,  $CH_3SO_2^+$ ,  $CH_4SO_3^+$ ,  $CH_3S^+$ ,  $C_3H_5SO_2^+$ , and  $C_4H_5SO_2^+$ .  
189 Previous studies have shown that  $CH_2SO_2^+$ ,  $CH_3SO_2^+$ , and  $CH_4SO_3^+$  are HR-AMS signature ions for methanesulfonic  
190 acid (MSA) (Ge et al., 2012). In this study, the three ions correlate ( $r = 0.50 - 0.71$ ; Fig. S10) with signal ratios close  
191 to those observed for pure methanesulfonic acid (Ge et al., 2012). This is an indication that mesylate ( $CH_3SO_3^-$ , the  
192 deprotonated anion of MSA) was present in the regional background aerosols in the western US. Based on the  
193 fragmentation pattern of MSA, where  $CH_3SO_2^+$  intensity contributed 8.7% to total MSA fragments in the HR-AMS  
194 (Ge et al., 2012), we estimated that the average MSA mass concentration was  $6.7 (\pm 7.2) \text{ ng m}^{-3}$ , making up  $\sim 0.3\%$   
195 of the total OA mass during the clean periods.

196 Oceans are generally considered dominant sources of dimethyl sulfide (DMS) and therefore its oxidation product  
197 MSA. However, the Pacific Ocean is 195 km to the west of MBO whereas the bivariate polar plot of MSA revealed  
198 that high concentrations were associated with winds from the east and the south (Fig. S11). This is an indication that  
199 the sources of MSA were mostly continental. In addition, MSA concentrations showed a clear diurnal cycle with a  
200 substantial daytime increase (Fig. 2), which suggests significant sources from the PBL. Aerosols in the PBL over this  
201 region likely have negligible oceanic influences since the Cascades mountain range lies between the Pacific Ocean  
202 and Mt. Bachelor and may obstruct surface wind bringing marine emissions inland. DMS can be emitted from a wide  
203 range of terrestrial sources including soil, vegetation, freshwater wetland, and paddy fields (Watts, 2000 and referencer  
204 therein). Furthermore, the maximum  $MSA/SO_4$  ratio was approximately 0.081, much lower than those observed in  
205 marine aerosols (e.g., average = 0.23 in sub-Arctic North East Pacific Ocean; (Phinney et al., 2006)). The  $MSA/SO_4$   
206 ratios are much lower in terrestrial regions, e.g., 0.01 - 0.17 in Fresno where MSA was attributed to non-marine sources  
207 (Ge et al., 2012; Young et al., 2016) and 0.007 - 0.15 along the Atlantic coast under continental influences (Zorn et  
208 al., 2008; Huang et al., 2017).

### 209 3.3. Sources and Processes of Aerosols in the Remote Region of the Western US

210 PMF analysis was performed on the NR- $PM_1$  mass spectra acquired during the clean periods to further elucidate  
211 the sources and processes of the regional background aerosols observed at MBO. Two OA factors were identified,  
212 including an intermediately oxidized, semi-volatile OOA (SV-OOA,  $O/C = 0.67$ ;  $H/C = 1.57$ ) and a highly oxidized,  
213 low volatility OOA (LV-OOA,  $O/C = 1.17 \pm 0.08$ ;  $H/C = 1.18 \pm 0.03$ ). No hydrocarbon-like (HOA) factor was



214 identified during the clean periods, which is consistent with a low abundance of  $C_4H_9^+$  signal (0.13% of total OA  
215 signal), a tracer ion for primary OA from vehicle emissions (Collier et al., 2015). In addition,  $f_{60}$  was constantly lower  
216 than 0.3% (Fig. S6 and Fig. S13b), indicating a lack of BB influence (Cubison et al., 2011). These results indicate the  
217 absence of primary aerosol sources at MBO during clean periods.

218 SV-OOA, which on average accounted for 70% of total OA mass at MBO during clean periods (Fig. 3c), showed  
219 temporal features that indicate a strong influence from BL dynamics. Particularly, SV-OOA correlated well with CO,  
220 nitrate, and MSA ( $r = 0.7 - 0.84$ ) and exhibited a pronounced diurnal cycle that increases between 9:00 – 10:00, peaks  
221 around 15:30 (PST), and decreases to a very low concentration ( $\sim 0.1 \mu\text{g m}^{-3}$ ) at night (Fig. 2). The SV-OOA mass  
222 spectrum displayed the characteristics of secondary OA (SOA) with two dominant oxygenated ions,  $C_2H_3O^+$  ( $m/z =$   
223  $43.018$ ) and  $CO_2^+$  ( $m/z = 43.989$ ) (Fig. 3a). The signal intensity of  $C_2H_3O^+$  is similar to that of  $CO_2^+$  and the SV-OOA  
224 spectrum comprises relatively abundant  $C_xH_y^+$  and  $C_xH_yO_1^+$  ions (Fig. 3a). These features, as well as an average O/C  
225 of 0.67, indicate that SV-OOA was moderately oxidized and was likely not very aged.

226 The SV-OOA spectrum showed a significant  $C_7H_7^+$  signal ( $m/z = 91.055$ ), which was proposed as an indicator  
227 for the presence of  $\beta$ -pinene +  $NO_3$  reaction products (Boyd et al., 2015). Elevated  $C_7H_7^+$  is an AMS spectral feature  
228 for biogenic SOA observed both in ambient air and in chambers experiments (Kiendler-Scharr et al., 2009; Sun et al.,  
229 2009; Robinson et al., 2011; Setyan et al., 2012; Budisulistiorini et al., 2015; Chen et al., 2015). In fact, the SV-OOA  
230 spectrum of this study is highly similar to the spectra of biogenic SOA observed previously in both laboratory and  
231 field studies. These findings as well as the fact that organonitrates were predominantly associated with SV-OOA (Fig.  
232 S12) indicate that the SV-OOA observed in this study likely represented biogenic SOA formed at lower altitudes in  
233 the region and transported upward to the site by thermal winds during the day.

234 LV-OOA, which accounted for an average 30% of total OA mass, likely represented more aged SOA in the  
235 regional background air. It exhibited a much less pronounced diurnal trend than SV-OOA (Fig. 2) and presented as a  
236 major OA component during most nights when the site was in the FT (Fig. 1g). These results suggest that LV-OOA  
237 likely represents OA in the FT, which can be long-distance transported and/or regionally recirculated due to longer  
238 aerosol lifetime and higher wind speed in the FT. LV-OOA was highly oxidized with an average O/C of 1.17 (Fig.  
239 3b) and contributed major fractions of highly oxygenated organic ions, e.g.,  $C_4H_3O_3^+$ ,  $C_3H_5O_3^+$ , and  $C_6H_5O_3^+$ , and  
240  $CO_2^+$  and  $CHO_2^+$  – HR-AMS signature ions for carboxylic acids (Fig. 3e). In contrast, nearly all the  $C_8H_{11}^+$ ,  $C_6H_{11}O^+$ ,  
241  $C_5H_9^+$  and  $C_3H_7^+$  signals were attributed to SV-OOA, so were a majority of the  $C_4H_7^+$  (91%) and  $C_2H_3O^+$  (86%) signals  
242 (Fig. 3d and 3e). In addition, LV-OOA was tightly associated with sulfate (Fig. 3b and 3e), a secondary aerosol species  
243 representative of aged, regional air masses. Furthermore, LV-OOA situates near the apex of the triangle region for  
244 ambient OAs in the  $f_{44}$  vs  $f_{43}$  space (Fig. S13a), overlapping with the highly oxidized LV-OOA observed in various  
245 environments (Ng et al., 2010) as well as highly aged OAs observed at high altitude (Sun et al., 2009; Fröhlich et  
246 al., 2015). These results together suggest that LV-OOA likely represented free tropospheric SOA in the western U.S  
247 and were composed of highly oxidized organic compounds.



### 248 3.4 Differences between Aerosols in BL and FT Air Masses

249 Because MBO tends to sample the free troposphere air at night and the regional boundary layer air during the  
250 day, the measurement data are used to examine the differences between aerosols in both parts of the atmosphere during  
251 clean periods. Extensive work has been done to differentiate free tropospheric air from boundary layer-influenced air  
252 at MBO using water vapor chairlift soundings (Reidmiller et al., 2010) and other approaches (Weiss-Penzias et al.,  
253 2006; Fischer et al., 2010; Ambrose et al., 2011; McClure et al., 2016; Zhang and Jaffe, 2017). Zhang and Jaffe (2017)  
254 contributed to a more accurate monthly FT/BL-influence isolation at MBO based on comparison of MBO  $\text{H}_2\text{O}_{(\text{g})}$   
255 distributions to the  $\text{H}_2\text{O}_{(\text{g})}$  soundings from Medford and Salem, Oregon, at equivalent pressure level. Based on this  
256 work we classify periods with  $\text{H}_2\text{O}_{(\text{g})}$  above the minimum monthly water vapor criteria value,  $2.5 \text{ g kg}^{-1}$ , and  $\text{CO} > 80$   
257 ppb as those dominated by “BL-influenced air” and the rest by “FT air”. A discussion on the comparison between this  
258 method and using the estimated BL height as the differentiating criteria can be found in Section 1 of the Supplement.

259 The average concentration of NR- $\text{PM}_{10}$  under BL influences was  $3.16 \mu\text{g m}^{-3}$ , approximately 4 times of that in  
260 the FT ( $0.85 \mu\text{g m}^{-3}$ ). While OA mass was on average 6 times higher in the BL than in the FT ( $2.7$  vs  $0.34 \mu\text{g m}^{-3}$ ),  
261 sulfate mass concentrations in these two types of air masses were similar ( $0.35$  vs  $0.33 \mu\text{g m}^{-3}$ ). The stoichiometric  
262 neutralization of the inorganic components of NR- $\text{PM}_{10}$  was examined by comparing the molar equivalent ratio of  
263 ammonium ( $[\text{NH}_4^+]/18$ ) and sulfate ( $[\text{SO}_4^{2-}]/48$ ) since inorganic nitrate and chloride concentrations appeared to be  
264 negligible during clean periods. The ammonium-to-sulfate equivalent ratios in aerosols during clean periods varied  
265 between  $0.005 - 1$  (Fig. 4a), indicating that remote aerosols in the western US were frequently acidic in the summer.  
266 Most significant is that a substantial amount of FT aerosols ( $\sim 78\%$  of FT NR- $\text{PM}_{10}$  mass vs  $16\%$  of BL NR- $\text{PM}_{10}$  mass)  
267 exhibited an ammonium-to-sulfate equivalent ratio lower than  $0.3$  (Fig. 4a), indicating the presence of very acidic  
268 particles in the free troposphere. Acidic FT particles were also observed at various high-altitude regional background  
269 sites, such as Jungfraujoch (Cozic et al., 2008; Fröhlich et al., 2015), Puy de Dome station (Frenay et al., 2016),  
270 Whistler mountain (Sun et al., 2009), and Mauna Loa (Hawaii, US) (Johnson and Kumar, 1991), and during airborne  
271 measurements in the upper troposphere of the tropics (Froyd et al., 2009) and the Arctic (Brock et al., 2011; Fisher et  
272 al., 2011).

273 MSA correlated with HR-AMS sulfate for different aerosol regimes with different slopes. As shown in Fig. 4b,  
274 BL-influenced aerosols showed a range of MSA/ $\text{SO}_4$  ratios generally higher than FT aerosols, possibly owing to  
275 relatively abundant sulfate particles in the FT. When a polluted air mass is lifted out of the boundary layer, the already  
276 formed aerosol can be washed out due to precipitation during lifting while the less-soluble gas phase compounds such  
277 as  $\text{SO}_2$  are not entirely removed. The resulting gas phase mixture is then relatively enhanced in  $\text{SO}_2$ . Consequently,  
278 during the subsequent regional transport in the FT, sulfate forms in larger concentrations than MSA.

279 In addition to aerosol chemical properties, the physical properties of MBO aerosols were examined. The average  
280 mass-based size distribution of NR- $\text{PM}_{10}$  during the clean periods displayed a broad feature extending from  $100$  to  
281  $1000 \text{ nm}$  in vacuum aerodynamic diameter ( $D_{\text{va}}$ , Fig. 5). Aerosol composition varied as a function of size with larger  
282 particles ( $>200 \text{ nm}$ ) having a relatively larger sulfate contribution ( $12\%$ ) compared to smaller particles ( $<5\%$ ). Org43,  
283 the organic signal at  $m/z = 43$  ( $90\%$  of which was  $\text{C}_2\text{H}_3\text{O}^+$ ), presented a broad distribution peaking between  $250$  and  
284  $350 \text{ nm}$  in  $D_{\text{va}}$  (Fig. 5b). In contrast, Org44, the organic signal at  $m/z = 44$  ( $95\%$  of which was  $\text{CO}_2^+$ ), and sulfate



285 displayed distinctly narrower distributions peaking at a larger droplet accumulation mode close to 500 nm (Fig. 5b  
286 and 5c). The similar size distribution of Org44 and sulfate and the tight correlation between their concentrations ( $r^2 =$   
287 0.61; Fig. S14) suggest that highly oxidized organics and sulfate had similar sources and processes and are possibly  
288 internally mixed. In particular, the prominent droplet mode at 500 nm indicates an important influence of aqueous-  
289 phase reactions on the production of sulfate and highly oxidized organics. Indeed, previous studies have shown that  
290 aqueous-phase processing (i.e., fog and cloud droplets and aerosol phase water) have led to production of more  
291 oxidized organics (Lee et al., 2011; Lee et al., 2012; Ervens et al., 2013) in the droplet mode (Ge et al., 2012) and  
292 that aqueous-phase production of sulfate is an important process in the atmosphere (e.g., Ervens et al., 2011). In  
293 addition, a similar sulfate size distribution was observed at the peak of Whistler Mountain, which had frequent cloud  
294 cover (Sun et al., 2009).

295 A distinctly different size distribution was observed for sulfate-containing particles in the FT, as shown in Fig  
296 5c, where it exhibited a prominent mode at  $\sim 250$  nm. One possible explanation is condensational growth of newly  
297 nucleated particles in the FT. Scavenging can significantly remove larger particles, resulting in low particle surface  
298 area that facilitates new particle formation (NPF) in the FT. Indeed, in-situ NPF events have been frequently observed  
299 in the FT at locations such as the Storm Peak Laboratory (Hallar et al., 2011; Hallar et al., 2013) and Jungfraujoch  
300 (Bianchi et al., 2016; Tröstl et al., 2016), and in clean areas such as Arctic (Tunved et al., 2013; Freud et al., 2017).  
301 The formation and growth of new particles has also been observed over a broad region in the FT (Tröstl et al., 2016).  
302 At MBO, daily thermal winds may have uplifted gas precursors from the BL to the FT, which can be further oxidized  
303 in the FT and then condensed onto new particles, leading to the condensational growth of particles (Bianchi et al.,  
304 2016). These observations shed light on the different sources and processes of aerosols in the BL and FT and suggest  
305 that sulfate and organic aerosols were likely present in variable mixtures (i.e., both internal and external mixtures) at  
306 MBO.

### 307 3.5. Comparisons with Aerosols Observed at Other High-altitude Locations

308 Figure 6 summarizes the average composition of NR-PM<sub>1</sub> measured using AMS or Aerosol Chemical Speciation  
309 Monitors (ACSM) at various elevated regional background ground sites (Zhang et al., 2007; Sun et al., 2009; Freney  
310 et al., 2011; Worton et al., 2011; Fröhlich et al., 2015; Rinaldi et al., 2015; Schurman et al., 2015; Freney et al., 2016;  
311 Zhu et al., 2016; Xu et al., 2018) and by aircraft (Bahreini et al., 2003; Dunlea et al., 2009). All of these measurements  
312 were conducted under conditions absent of biomass burning influence and representative of regional background  
313 aerosols in the northern hemisphere. Mountain-top studies separated FT air based on BLH calculated from LIDAR  
314 measurements (Freney et al., 2016) or tracers such as <sup>222</sup>Rn concentrations and NO<sub>y</sub>/CO and back trajectory analysis  
315 (Fröhlich et al., 2015). The average NR-PM<sub>1</sub> mass concentrations across all sites was 5.1 ( $\pm 6.9$ )  $\mu\text{g m}^{-3}$  and the value  
316 in North America was 2.6 ( $\pm 1.6$ )  $\mu\text{g m}^{-3}$ . NR-PM<sub>1</sub> concentrations were, on average, substantially lower in the FT than  
317 in the BL influenced air ( $0.68 \pm 0.18 \mu\text{g m}^{-3}$  v.s.  $5.8 \pm 7.3 \mu\text{g m}^{-3}$ ), reflecting generally clean conditions in the FT.

318 A major fraction (27 – 84%; average = 51%) of the NR-PM<sub>1</sub> mass was organic matter at these remote high-  
319 altitude locations (Fig. 6a). For the same site, marked chemical difference can be seen between aerosols in the FT and  
320 the BL. At all sites, FT aerosols contained a substantially higher mass fraction of sulfate (39 – 44%) compared to the



321 mixed BL/FT aerosols (11 – 35%). Aircraft measurements also showed consistent results of higher sulfate content in  
322 aerosols at higher altitudes. For example, Bahreini et al. (2003) reported that the sulfate contribution to total NR-PM<sub>1</sub>  
323 over east Asia increased from 17.4% in the lower atmosphere (1-3 km) to 28.8% in layers > 3 km. In the FT over the  
324 northeast Pacific, more than half of the background submicron mass was attributed to sulfate (Dunlea et al., 2009;  
325 Roberts et al., 2010). Elevated sulfate layers were also clearly observed in the higher altitudes above Mexico City  
326 (DeCarlo et al., 2008). As a result, the mass ratio of submicron sulfate to organics (SO<sub>4</sub>/Org) showed significantly  
327 higher values (0.72 to 1.1) in the FT air masses than those in the mixed layers (0.13 – 0.7; Fig. 6b)

328 The extent to which sulfate particles are neutralized has major implications for aerosol radiative forcing. The  
329 average relative humidity at MBO was 25.6 (±8.9) % during the clean periods. Acidic sulfate aerosols are more  
330 hygroscopic than ammonium sulfate (Taylor et al., 2017), thus uptake of gaseous ammonia by acidic particles may  
331 produce solid ammonium sulfate at low relative humidity. The resulting decrease in aerosol water content both reduces  
332 the direct radiative forcing of sulfate (Adams et al., 2001; Jacobson, 2001) and inhibits homogenous ice nucleation by  
333 liquid sulfate-containing particles (Koop et al., 2000). In addition, solid ammonium sulfate aerosols can also be  
334 effective heterogeneous ice nuclei for cirrus cloud formation (Abbatt et al., 2006). While mineral dust particles coated  
335 with ammonium sulfate are efficient ice nuclei, those coated with sulfuric acid can lose their ice nucleating ability  
336 (Eastwood et al., 2009).

#### 337 4. Summary and Conclusions

338 Based on field observations at a remote high-altitude atmospheric research station - the Mt. Bachelor Observatory  
339 (MBO, 43.98° N, 121.69° W, 2763 m a.s.l.) in central Oregon - we have characterized the chemical and physical  
340 properties of aerosols in the boundary layer and free troposphere air under clean conditions in the absence of wildfire  
341 influences in the western US. Water vapor mixing ratio, a tracer used to segregate FT and BL-influenced air masses  
342 at MBO, showed a strong diurnal cycle. Dry free tropospheric conditions were frequently observed at night, whereas  
343 humid boundary layer influenced air was often observed during the day. The average (± 1σ) NR-PM<sub>1</sub> mass  
344 concentration during the entire clean period was 2.8 (± 2.8) μg m<sup>-3</sup>, with OA dominating the NR-PM<sub>1</sub> composition (~  
345 84%) followed by sulfate (11%). OA, nitrate, and MSA displayed clear diurnal cycles with substantial daytime  
346 increases, suggesting significantly higher mass concentrations in the BL than in the FT.

347 Strong diurnal patterns driven by the boundary layer dynamics were also observed in aerosol chemical  
348 composition. NR-PM<sub>1</sub> contained a significantly higher mass fraction of sulfate (up to 83% of NR-PM<sub>1</sub> mass) and was  
349 frequently acidic at night when MBO resided in the FT. In addition, nighttime free tropospheric OA was found to be  
350 more oxidized. PMF analysis identified two types of OOA representing the regional background OA in the western  
351 US: a LV-OOA (30% of OA mass) that was highly oxidized (O/C = 1.17) and comprised of low-volatility organics,  
352 representative of SOA in the free troposphere; and an SV-OOA (70% of OA mass) that was intermediately oxidized  
353 (O/C = 0.67) and appeared to be semivolatile, representative of biogenic SOA in the BL. NR-PM<sub>1</sub> observed at other  
354 high-altitude locations in the world under regional background conditions were summarized. These results highlight  
355 the significant compositional differences between FT and BL aerosols in that the FT aerosols are significantly more



356 oxidized and contain a higher fraction of sulfate. These observations may have important implications for  
357 understanding the climate effects of aerosols in remote regions.

#### 358 **Data availability**

359 Data presented in this manuscript are available upon request to the corresponding author.

#### 360 **Acknowledgements**

361 This work is supported by US Department of Energy Atmospheric System Research Program, Grant No. DE-  
362 SC0014620. Shan Zhou acknowledges funding from the Chinese Scholarship Council (CSC) and the Donald G.  
363 Crosby Fellowship and the Fumio Matsumura Memorial Fellowship from the University of California at Davis. The  
364 Mt. Bachelor Observatory is supported by the National Science Foundation (grant #AGS-1447832) and the National  
365 Oceanic and Atmospheric Administration (contract #RA-133R-16-SE-0758).

#### 366 **References**

- 367 Abbatt, J. P. D., Benz, S., Cziczo, D. J., Kanji, Z., Lohmann, U., and Möhler, O.: Solid Ammonium Sulfate Aerosols  
368 as Ice Nuclei: A Pathway for Cirrus Cloud Formation, *Science*, 313, 1770-1773, 2006.
- 369 Adams, P. J., Seinfeld, J. H., Koch, D., Mickley, L., and Jacob, D.: General circulation model assessment of direct  
370 radiative forcing by the sulfate-nitrate-ammonium-water inorganic aerosol system, *J. Geophys. Res. Atmos.*, 106,  
371 1097-1111, 2001.
- 372 Aiken, A. C., Decarlo, P. F., Kroll, J. H., Worsnop, D. R., Huffman, J. A., Docherty, K. S., Ulbrich, I. M., Mohr, C.,  
373 Kimmel, J. R., Sueper, D., Sun, Y., Zhang, Q., Trimborn, A., Northway, M., Ziemann, P. J., Canagaratna, M. R.,  
374 Onasch, T. B., Alfarra, M. R., Prevot, A. S. H., Dommen, J., Duplissy, J., Metzger, A., Baltensperger, U., and  
375 Jimenez, J. L.: O/C and OM/OC ratios of primary, secondary, and ambient organic aerosols with high-resolution  
376 time-of-flight aerosol mass spectrometry, *Environ. Sci. Tech.*, 42, 4478-4485, 2008.
- 377 Ambrose, J. L., Reidmiller, D. R., and Jaffe, D. A.: Causes of high O<sub>3</sub> in the lower free troposphere over the Pacific  
378 Northwest as observed at the Mt. Bachelor Observatory, *Atmos. Environ.*, 45, 5302-5315, 2011.
- 379 Bahreini, R., Jimenez, J. L., Wang, J., Flagan, R. C., Seinfeld, J. H., Jayne, J. T., and Worsnop, D. R.: Aircraft-based  
380 aerosol size and composition measurements during ACE-Asia using an Aerodyne aerosol mass spectrometer, *J.*  
381 *Geophys. Res. Atmos.*, 108, 8645, 2003.
- 382 Bianchi, F., Trostl, J., Junninen, H., Frege, C., Henne, S., Hoyle, C. R., Molteni, U., Herrmann, E., Adamov, A.,  
383 Bukowiecki, N., Chen, X., Duplissy, J., Gysel, M., Hutterli, M., Kangasluoma, J., Kontkanen, J., Kurten, A.,  
384 Manninen, H. E., Munch, S., Perakyla, O., Petaja, T., Rondo, L., Williamson, C., Weingartner, E., Curtius, J.,  
385 Worsnop, D. R., Kulmala, M., Dommen, J., and Baltensperger, U.: New particle formation in the free troposphere:  
386 A question of chemistry and timing, *Science*, 352, 1109-1112, 2016.



- 387 Bolton, D.: The Computation of Equivalent Potential Temperature, *Monthly Weather Review*, 108, 1046-1053,  
388 1980.
- 389 Boucher, O., D. Randall, P. Artaxo, C. Bretherton, G. Feingold, P. Forster, V.-M. Kerminen, Y. Kondo, H. Liao, U.  
390 Lohmann, P. Rasch, S.K. Satheesh, S. Sherwood, B. Stevens and X.Y. Zhang: Clouds and Aerosols. In: *Climate*  
391 *Change 2013: The Physical Science Basis. Contribution of Working Group I to the Fifth Assessment Report of the*  
392 *Intergovernmental Panel on Climate Change*, Cambridge University Press, Cambridge, United Kingdom and New  
393 York, NY, USA., 2013.
- 394 Boyd, C. M., Sanchez, J., Xu, L., Eugene, A. J., Nah, T., Tuet, W. Y., Guzman, M. I., and Ng, N. L.: Secondary  
395 organic aerosol formation from the  $\beta$ -pinene+NO<sub>3</sub> system: effect of humidity and peroxy radical fate, *Atmos.*  
396 *Chem. Phys.*, 15, 7497-7522, 2015.
- 397 Briggs, N. L., Jaffe, D. A., Gao, H., Hee, J. R., Baylon, P. M., Zhang, Q., Zhou, S., Collier, S. C., Sampson, P. D.,  
398 and Cary, R. A.: Particulate Matter, Ozone, and Nitrogen Species in Aged Wildfire Plumes Observed at the Mount  
399 Bachelor Observatory, *Aerosol Air Qual. Res.*, 16, 3075-3087, 2016.
- 400 Brock, C. A., Cozic, J., Bahreini, R., Froyd, K. D., Middlebrook, A. M., McComiskey, A., Brioude, J., Cooper, O.  
401 R., Stohl, A., Aikin, K. C., de Gouw, J. A., Fahey, D. W., Ferrare, R. A., Gao, R. S., Gore, W., Holloway, J. S.,  
402 Hübler, G., Jefferson, A., Lack, D. A., Lance, S., Moore, R. H., Murphy, D. M., Nenes, A., Novelli, P. C., Nowak, J.  
403 B., Ogren, J. A., Peischl, J., Pierce, R. B., Pilewskie, P., Quinn, P. K., Ryerson, T. B., Schmidt, K. S., Schwarz, J. P.,  
404 Sodemann, H., Spackman, J. R., Stark, H., Thomson, D. S., Thornberry, T., Veres, P., Watts, L. A., Warneke, C.,  
405 and Wollny, A. G.: Characteristics, sources, and transport of aerosols measured in spring 2008 during the aerosol,  
406 radiation, and cloud processes affecting Arctic Climate (ARCPAC) Project, *Atmos. Chem. Phys.*, 11, 2423-2453,  
407 2011.
- 408 Budisulistiorini, S. H., Li, X., Bairai, S. T., Renfro, J., Liu, Y., Liu, Y. J., McKinney, K. A., Martin, S. T., McNeill,  
409 V. F., Pye, H. O. T., Nenes, A., Neff, M. E., Stone, E. A., Mueller, S., Knote, C., Shaw, S. L., Zhang, Z., Gold, A.,  
410 and Surratt, J. D.: Examining the effects of anthropogenic emissions on isoprene-derived secondary organic aerosol  
411 formation during the 2013 Southern Oxidant and Aerosol Study (SOAS) at the Look Rock, Tennessee ground site,  
412 *Atmos. Chem. Phys.*, 15, 8871-8888, 2015.
- 413 Canagaratna, M. R., Jimenez, J. L., Kroll, J. H., Chen, Q., Kessler, S. H., Massoli, P., Hildebrandt Ruiz, L., Fortner,  
414 E., Williams, L. R., Wilson, K. R., Surratt, J. D., Donahue, N. M., Jayne, J. T., and Worsnop, D. R.: Elemental ratio  
415 measurements of organic compounds using aerosol mass spectrometry: characterization, improved calibration, and  
416 implications, *Atmos. Chem. Phys.*, 15, 253-272, 2015.
- 417 Chen, Q., Farmer, D. K., Rizzo, L. V., Pauliquevis, T., Kuwata, M., Karl, T. G., Guenther, A., Allan, J. D., Coe, H.,  
418 Andreae, M. O., Pöschl, U., Jimenez, J. L., Artaxo, P., and Martin, S. T.: Submicron particle mass concentrations  
419 and sources in the Amazonian wet season (AMAZE-08), *Atmos. Chem. Phys.*, 15, 3687-3701, 2015.
- 420 Collier, S. and Zhang, Q.: Gas-Phase CO<sub>2</sub> Subtraction for Improved Measurements of the Organic Aerosol Mass  
421 Concentration and Oxidation Degree by an Aerosol Mass Spectrometer, *Environ. Sci. Tech.*, 47, 14324-14331,  
422 2013.
- 423 Collier, S., Zhou, S., Kuwayama, T., Forestieri, S., Brady, J., Zhang, M., Kleeman, M., Cappa, C., Bertram, T., and  
424 Zhang, Q.: Organic PM Emissions from Vehicles: Composition, O/C Ratio, and Dependence on PM Concentration,  
425 *Aerosol Sci. Tech.*, 49, 86-97, 2015.



- 426 Collier, S., Zhou, S., Onasch, T. B., Jaffe, D. A., Kleinman, L., Sedlacek, A. J., Briggs, N. L., Hee, J., Fortner, E.,  
427 Shilling, J. E., Worsnop, D., Yokelson, R. J., Parworth, C., Ge, X., Xu, J., Butterfield, Z., Chand, D., Dubey, M. K.,  
428 Pekour, M. S., Springston, S., and Zhang, Q.: Regional Influence of Aerosol Emissions from Wildfires Driven by  
429 Combustion Efficiency: Insights from the BBOP Campaign, *Environ. Sci. Tech.*, 50, 8613-8622, 2016.
- 430 Cozic, J., Verheggen, B., Weingartner, E., Crosier, J., Bower, K. N., Flynn, M., Coe, H., Henning, S., Steinbacher,  
431 M., Henne, S., Collaud Coen, M., Petzold, A., and Baltensperger, U.: Chemical composition of free tropospheric  
432 aerosol for PM<sub>1</sub> and coarse mode at the high alpine site Jungfraujoch, *Atmos. Chem. Phys.*, 8, 407-423, 2008.
- 433 Cubison, M. J., Ortega, A. M., Hayes, P. L., Farmer, D. K., Day, D., Lechner, M. J., Brune, W. H., Apel, E., Diskin,  
434 G. S., Fisher, J. A., Fuelberg, H. E., Hecobian, A., Knapp, D. J., Mikoviny, T., Riemer, D., Sachse, G. W., Sessions,  
435 W., Weber, R. J., Weinheimer, A. J., Wisthaler, A., and Jimenez, J. L.: Effects of aging on organic aerosol from  
436 open biomass burning smoke in aircraft and laboratory studies, *Atmos. Chem. Phys.*, 11, 12049-12064, 2011.
- 437 DeCarlo, P. F., Dunlea, E. J., Kimmel, J. R., Aiken, A. C., Sueper, D., Crounse, J., Wennberg, P. O., Emmons, L.,  
438 Shinozuka, Y., Clarke, A., Zhou, J., Tomlinson, J., Collins, D. R., Knapp, D., Weinheimer, A. J., Montzka, D. D.,  
439 Campos, T., and Jimenez, J. L.: Fast airborne aerosol size and chemistry measurements above Mexico City and  
440 Central Mexico during the MILAGRO campaign, *Atmos. Chem. Phys.*, 8, 4027-4048, 2008.
- 441 Draxler, R. R., Hess, G. D. : An overview of the Hysplit-4 modeling system for trajectories, dispersion, and  
442 deposition, *Aust. Meteorol. Magn.*, 47, 295-308, 1998.
- 443 Dunlea, E. J., DeCarlo, P. F., Aiken, A. C., Kimmel, J. R., Peltier, R. E., Weber, R. J., Tomlinson, J., Collins, D. R.,  
444 Shinozuka, Y., McNaughton, C. S., Howell, S. G., Clarke, A. D., Emmons, L. K., Apel, E. C., Pfister, G. G., van  
445 Donkelaar, A., Martin, R. V., Millet, D. B., Heald, C. L., and Jimenez, J. L.: Evolution of Asian aerosols during  
446 transpacific transport in INTEX-B, *Atmos. Chem. Phys.*, 9, 7257-7287, 2009.
- 447 Dzepina, K., Mazzoleni, C., Fialho, P., China, S., Zhang, B., Owen, R. C., Helmig, D., Hueber, J., Kumar, S.,  
448 Perlinger, J. A., Kramer, L. J., Dziobak, M. P., Ampadu, M. T., Olsen, S., Wuebbles, D. J., and Mazzoleni, L. R.:  
449 Molecular characterization of free tropospheric aerosol collected at the Pico Mountain Observatory: a case study  
450 with a long-range transported biomass burning plume, *Atmos. Chem. Phys.*, 15, 5047-5068, 2015.
- 451 Eastwood, M. L., Cremel, S., Wheeler, M., Murray, B. J., Girard, E., and Bertram, A. K.: Effects of sulfuric acid and  
452 ammonium sulfate coatings on the ice nucleation properties of kaolinite particles, *Geophys Res Lett*, 36, L02811,  
453 2009.
- 454 Ervens, B., Turpin, B. J., and Weber, R. J.: Secondary organic aerosol formation in cloud droplets and aqueous  
455 particles (aqSOA): a review of laboratory, field and model studies, *Atmos. Chem. Phys.*, 11, 11069-11102, 2011.
- 456 Ervens, B., Wang, Y., Eagar, J., Leaitch, W. R., Macdonald, A. M., Valsaraj, K. T., and Herckes, P.: Dissolved  
457 organic carbon (DOC) and select aldehydes in cloud and fog water: the role of the aqueous phase in impacting trace  
458 gas budgets, *Atmos. Chem. Phys.*, 13, 5117-5135, 2013.
- 459 Farmer, D. K., Matsunaga, A., Docherty, K. S., Surratt, J. D., Seinfeld, J. H., Ziemann, P. J., and Jimenez, J. L.:  
460 Response of an aerosol mass spectrometer to organonitrates and organosulfates and implications for atmospheric  
461 chemistry, *P. Natl. Acad. Sci. USA*, 107, 6670-6675, 2010.
- 462 Fischer, E. V., Jaffe, D. A., Reidmiller, D. R., and Jaegle, L.: Meteorological controls on observed peroxyacetyl  
463 nitrate at Mount Bachelor during the spring of 2008, *J. Geophys. Res. Atmos.*, 115, 2010.



- 464 Fischer, E. V., Jaffe, D. A., and Weatherhead, E. C.: Free tropospheric peroxyacetyl nitrate (PAN) and ozone at  
465 Mount Bachelor: potential causes of variability and timescale for trend detection, *Atmos. Chem. Phys.*, 11, 5641-  
466 5654, 2011.
- 467 Fisher, J. A., Jacob, D. J., Wang, Q., Bahreini, R., Carouge, C. C., Cubison, M. J., Dibb, J. E., Diehl, T., Jimenez, J.  
468 L., Leibensperger, E. M., Lu, Z., Meinders, M. B. J., Pye, H. O. T., Quinn, P. K., Sharma, S., Streets, D. G., van  
469 Donkelaar, A., and Yantosca, R. M.: Sources, distribution, and acidity of sulfate–ammonium aerosol in the Arctic in  
470 winter–spring, *Atmos. Environ.*, 45, 7301-7318, 2011.
- 471 Freney, E., Sellegri, K., Asmi, E., Rose, C., Chauvigne, A., Baray, J. L., Colomb, A., Hervo, M., Montoux, N.,  
472 Bouvier, L., and Picard, D.: Experimental Evidence of the Feeding of the Free Troposphere with Aerosol Particles  
473 from the Mixing Layer, *Aerosol Air Qual. Res.*, 16, 702-716, 2016.
- 474 Freney, E. J., Sellegri, K., Canonaco, F., Boulon, J., Hervo, M., Weigel, R., Pichon, J. M., Colomb, A., Prévôt, A. S.  
475 H., and Laj, P.: Seasonal variations in aerosol particle composition at the puy-de-Dôme research station in France,  
476 *Atmos. Chem. Phys.*, 11, 13047-13059, 2011.
- 477 Freud, E., Krejci, R., Tunved, P., Leaitch, R., Nguyen, Q. T., Massling, A., Skov, H., and Barrie, L.: Pan-Arctic  
478 aerosol number size distributions: seasonality and transport patterns, *Atmos. Chem. Phys.*, 17, 8101-8128, 2017.
- 479 Fröhlich, R., Cubison, M. J., Slowik, J. G., Bukowiecki, N., Canonaco, F., Croteau, P. L., Gysel, M., Henne, S.,  
480 Herrmann, E., Jayne, J. T., Steinbacher, M., Worsnop, D. R., Baltensperger, U., and Prévôt, A. S. H.: Fourteen  
481 months of on-line measurements of the non-refractory submicron aerosol at the Jungfraujoch (3580 m a.s.l.) –  
482 chemical composition, origins and organic aerosol sources, *Atmos. Chem. Phys.*, 15, 11373-11398, 2015.
- 483 Froyd, K. D., Murphy, D. M., Sanford, T. J., Thomson, D. S., Wilson, J. C., Pfister, L., and Lait, L.: Aerosol  
484 composition of the tropical upper troposphere, *Atmos. Chem. Phys.*, 9, 4363-4385, 2009.
- 485 Fry, J. L., Draper, D. C., Zarzana, K. J., Campuzano-Jost, P., Day, D. A., Jimenez, J. L., Brown, S. S., Cohen, R. C.,  
486 Kaser, L., Hansel, A., Cappellin, L., Karl, T., Roux, A. H., Turnipseed, A., Cantrell, C., Lefer, B. L., and Grossberg,  
487 N.: Observations of gas- and aerosol-phase organic nitrates at BEACHON-RoMBAS 2011, *Atmos. Chem. Phys.*, 13,  
488 8585-8605, 2013.
- 489 Fry, J. L., Kiendler-Scharr, A., Rollins, A. W., Wooldridge, P. J., Brown, S. S., Fuchs, H., Dube, W., Mensah, A.,  
490 dal Maso, M., Tillmann, R., Dorn, H. P., Brauers, T., and Cohen, R. C.: Organic nitrate and secondary organic  
491 aerosol yield from NO<sub>3</sub> oxidation of beta-pinene evaluated using a gas-phase kinetics/aerosol partitioning model,  
492 *Atmos. Chem. Phys.*, 9, 1431-1449, 2009.
- 493 Ge, X. L., Zhang, Q., Sun, Y. L., Ruehl, C. R., and Setyan, A.: Effect of aqueous-phase processing on aerosol  
494 chemistry and size distributions in Fresno, California, during wintertime, *Environ. Chem.*, 9, 221-235, 2012.
- 495 Hallar, A. G., Lowenthal, D. H., Chirokova, G., Borys, R. D., and Wiedinmyer, C.: Persistent daily new particle  
496 formation at a mountain-top location, *Atmos. Environ.*, 45, 4111-4115, 2011.
- 497 Hallar, A. G., Lowenthal, D. H., Clegg, S. L., Samburova, V., Taylor, N., Mazzoleni, L. R., Zielinska, B. K.,  
498 Kristensen, T. B., Chirokova, G., McCubbin, I. B., Dodson, C., and Collins, D.: Chemical and hygroscopic  
499 properties of aerosol organics at Storm Peak Laboratory, *J. Geophys. Res. Atmos.*, 118, 4767-4779, 2013.



- 500 Hallar, A. G., Petersen, R., McCubbin, I. B., Lowenthal, D., Lee, S., Andrews, E., and Yu, F.: Climatology of New  
501 Particle Formation and Corresponding Precursors at Storm Peak Laboratory, *Aerosol Air Qual. Res.*, 16, 816-826,  
502 2016.
- 503 Huang, S., Poulain, L., van Pinxteren, D., van Pinxteren, M., Wu, Z., Herrmann, H., and Wiedensohler, A.:  
504 Latitudinal and Seasonal Distribution of Particulate MSA over the Atlantic using a Validated Quantification Method  
505 with HR-ToF-AMS, *Environ. Sci. Tech.*, 51, 418-426, 2017.
- 506 Jacobson, M. Z.: Global direct radiative forcing due to multicomponent anthropogenic and natural aerosols, *J.*  
507 *Geophys. Res. Atmos.*, 106, 1551-1568, 2001.
- 508 Jaffe, D., Prestbo, E., Swartzendruber, P., Weiss-Penzias, P., Kato, S., Takami, A., Hatakeyama, S., and Kajii, Y.:  
509 Export of atmospheric mercury from Asia, *Atmos. Environ.*, 39, 3029-3038, 2005a.
- 510 Jaffe, D., Tamura, S., and Harris, J.: Seasonal cycle and composition of background fine particles along the west  
511 coast of the US, *Atmos. Environ.*, 39, 297-306, 2005b.
- 512 Johnson, S. A. and Kumar, R.: Composition and spectral characteristics of ambient aerosol at Mauna Loa  
513 Observatory, *J. Geophys. Res. Atmos.*, 96, 5379-5386, 1991.
- 514 Kiendler-Scharr, A., Mensah, A. A., Friese, E., Topping, D., Nemitz, E., Prevot, A. S. H., Aijala, M., Allan, J.,  
515 Canonaco, F., Canagaratna, M., Carbone, S., Crippa, M., Dall'Osto, M., Day, D. A., De Carlo, P., Di Marco, C. F.,  
516 Elbern, H., Eriksson, A., Freney, E., Hao, L., Herrmann, H., Hildebrandt, L., Hillamo, R., Jimenez, J. L., Laaksonen,  
517 A., McFiggans, G., Mohr, C., O'Dowd, C., Otjes, R., Ovadnevaite, J., Pandis, S. N., Poulain, L., Schlag, P., Sellegri,  
518 K., Swietlicki, E., Tiitta, P., Vermeulen, A., Wahner, A., Worsnop, D., and Wu, H. C.: Ubiquity of organic nitrates  
519 from nighttime chemistry in the European submicron aerosol, *Geophys Res Lett*, 43, 7735-7744, 2016.
- 520 Kiendler-Scharr, A., Zhang, Q., Hohaus, T., Kleist, E., Mensah, A., Mentel, T. F., Spindler, C., Uerlings, R.,  
521 Tillmann, R., and Wildt, J.: Aerosol Mass Spectrometric Features of Biogenic SOA: Observations from a Plant  
522 Chamber and in Rural Atmospheric Environments, *Environ. Sci. Tech.*, 43, 8166-8172, 2009.
- 523 Koop, T., Luo, B., Tsias, A., and Peter, T.: Water activity as the determinant for homogeneous ice nucleation in  
524 aqueous solutions, *Nature*, 406, 611-614, 2000.
- 525 Kroll, J. H., Donahue, N. M., Jimenez, J. L., Kessler, S. H., Canagaratna, M. R., Wilson, K. R., Altieri, K. E.,  
526 Mazzoleni, L. R., Wozniak, A. S., Bluhm, H., Mysak, E. R., Smith, J. D., Kolb, C. E., and Worsnop, D. R.: Carbon  
527 oxidation state as a metric for describing the chemistry of atmospheric organic aerosol, *Nature Chemistry*, 3, 133-  
528 139, 2011.
- 529 Laing, J. R., Jaffe, D. A., and Hee, J. R.: Physical and optical properties of aged biomass burning aerosol from  
530 wildfires in Siberia and the Western USA at the Mt. Bachelor Observatory, *Atmos. Chem. Phys.*, 16, 15185-15197,  
531 2016.
- 532 Lee, A., Goldstein, A. H., Keywood, M. D., Gao, S., Varutbangkul, V., Bahreini, R., Ng, N. L., Flagan, R. C., and  
533 Seinfeld, J. H.: Gas-phase products and secondary aerosol yields from the ozonolysis of ten different terpenes, *J.*  
534 *Geophys. Res. Atmos.*, 111, D07302, 2006.



- 535 Lee, A. K. Y., Hayden, K. L., Herckes, P., Leaitch, W. R., Liggio, J., Macdonald, A. M., and Abbatt, J. P. D.:  
536 Characterization of aerosol and cloud water at a mountain site during WACS 2010: secondary organic aerosol  
537 formation through oxidative cloud processing, *Atmos. Chem. Phys.*, 12, 7103-7116, 2012.
- 538 Lee, A. K. Y., Herckes, P., Leaitch, W. R., Macdonald, A. M., and Abbatt, J. P. D.: Aqueous OH oxidation of  
539 ambient organic aerosol and cloud water organics: Formation of highly oxidized products, *Geophys Res Lett*, 38,  
540 L11805, 2011.
- 541 McClure, C. D., Jaffe, D. A., and Gao, H.: Carbon Dioxide in the Free Troposphere and Boundary Layer at the Mt.  
542 Bachelor Observatory, *Aerosol Air Qual. Res.*, 16, 717-728, 2016.
- 543 Middlebrook, A. M., Bahreini, R., Jimenez, J. L., and Canagaratna, M. R.: Evaluation of Composition-Dependent  
544 Collection Efficiencies for the Aerodyne Aerosol Mass Spectrometer using Field Data, *Aerosol Sci. Tech.*, 46, 258-  
545 271, 2012.
- 546 Ng, N. L., Brown, S. S., Archibald, A. T., Atlas, E., Cohen, R. C., Crowley, J. N., Day, D. A., Donahue, N. M., Fry,  
547 J. L., Fuchs, H., Griffin, R. J., Guzman, M. I., Herrmann, H., Hodzic, A., Iinuma, Y., Jimenez, J. L., Kiendler-  
548 Scharr, A., Lee, B. H., Luecken, D. J., Mao, J., McLaren, R., Mutzel, A., Osthoff, H. D., Ouyang, B., Picquet-  
549 Varrault, B., Platt, U., Pye, H. O. T., Rudich, Y., Schwantes, R. H., Shiraiwa, M., Stutz, J., Thornton, J. A., Tilgner,  
550 A., Williams, B. J., and Zaveri, R. A.: Nitrate radicals and biogenic volatile organic compounds: oxidation,  
551 mechanisms, and organic aerosol, *Atmos. Chem. Phys.*, 17, 2103-2162, 2017.
- 552 Ng, N. L., Canagaratna, M. R., Zhang, Q., Jimenez, J. L., Tian, J., Ulbrich, I. M., Kroll, J. H., Docherty, K. S.,  
553 Chhabra, P. S., Bahreini, R., Murphy, S. M., Seinfeld, J. H., Hildebrandt, L., Donahue, N. M., DeCarlo, P. F., Lanz,  
554 V. A., Prevot, A. S. H., Dinar, E., Rudich, Y., and Worsnop, D. R.: Organic aerosol components observed in  
555 Northern Hemispheric datasets from Aerosol Mass Spectrometry, *Atmos. Chem. Phys.*, 10, 4625-4641, 2010.
- 556 Paatero, P. and Tapper, U.: Positive Matrix Factorization - a Nonnegative Factor Model with Optimal Utilization of  
557 Error-Estimates of Data Values, *Environmetrics*, 5, 111-126, 1994.
- 558 Phinney, L., Richard Leaitch, W., Lohmann, U., Boudries, H., Worsnop, D. R., Jayne, J. T., Toom-Sauntry, D.,  
559 Wadleigh, M., Sharma, S., and Shantz, N.: Characterization of the aerosol over the sub-arctic north east Pacific  
560 Ocean, *Deep Sea Res. II: Top. Stud. Oceanogr*, 53, 2410-2433, 2006.
- 561 Reidmiller, D. R., Jaffe, D. A., Fischer, E. V., and Finley, B.: Nitrogen oxides in the boundary layer and free  
562 troposphere at the Mt. Bachelor Observatory, *Atmos. Chem. Phys.*, 10, 6043-6062, 2010.
- 563 Rinaldi, M., Gilardoni, S., Paglione, M., Sandrini, S., Fuzzi, S., Massoli, P., Bonasoni, P., Cristofanelli, P.,  
564 Marinoni, A., Poluzzi, V., and Decesari, S.: Organic aerosol evolution and transport observed at Mt. Cimone (2165  
565 m a.s.l.), Italy, during the PEGASOS campaign, *Atmos. Chem. Phys.*, 15, 11327-11340, 2015.
- 566 Roberts, G. C., Day, D. A., Russell, L. M., Dunlea, E. J., Jimenez, J. L., Tomlinson, J. M., Collins, D. R.,  
567 Shinozuka, Y., and Clarke, A. D.: Characterization of particle cloud droplet activity and composition in the free  
568 troposphere and the boundary layer during INTEX-B, *Atmos. Chem. Phys.*, 10, 6627-6644, 2010.
- 569 Robinson, N. H., Hamilton, J. F., Allan, J. D., Langford, B., Oram, D. E., Chen, Q., Docherty, K., Farmer, D. K.,  
570 Jimenez, J. L., Ward, M. W., Hewitt, C. N., Barley, M. H., Jenkin, M. E., Rickard, A. R., Martin, S. T., McFiggans,  
571 G., and Coe, H.: Evidence for a significant proportion of Secondary Organic Aerosol from isoprene above a  
572 maritime tropical forest, *Atmos. Chem. Phys.*, 11, 1039-1050, 2011.



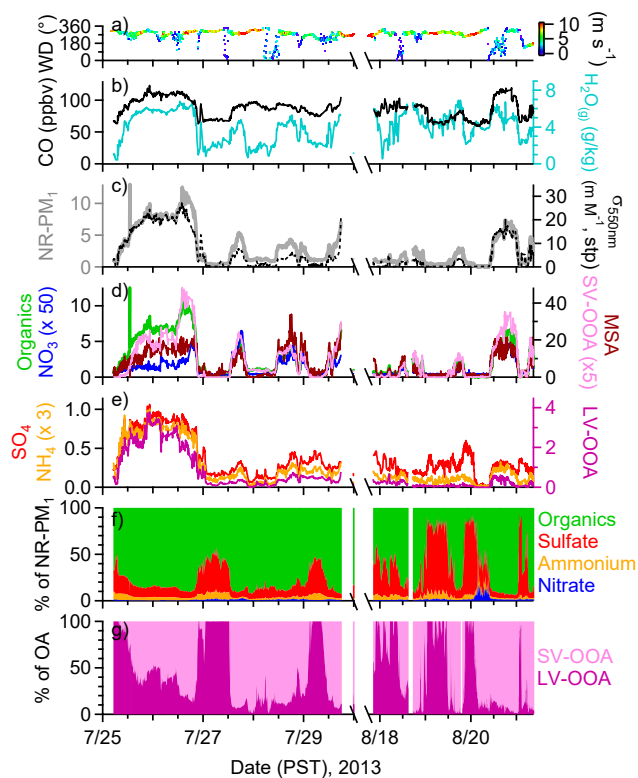
- 573 Rose, C., Sellegri, K., Asmi, E., Hervo, M., Freney, E., Colomb, A., Junninen, H., Duplissy, J., Sipilä, M.,  
574 Kontkanen, J., Lehtipalo, K., and Kulmala, M.: Major contribution of neutral clusters to new particle formation at  
575 the interface between the boundary layer and the free troposphere, *Atmos. Chem. Phys.*, 15, 3413-3428, 2015.
- 576 Schroder, F., Karcher, B., Fiebig, M., and Petzold, A.: Aerosol states in the free troposphere at northern  
577 midlatitudes, *J. Geophys. Res. Atmos.*, 107, 8126-8133, 2002.
- 578 Schurman, M. I., Lee, T., Sun, Y., Schichtel, B. A., Kreidenweis, S. M., and Collett Jr, J. L.: Investigating types and  
579 sources of organic aerosol in Rocky Mountain National Park using aerosol mass spectrometry, *Atmos. Chem. Phys.*,  
580 15, 737-752, 2015.
- 581 Setyan, A., Zhang, Q., Merkel, M., Knighton, W. B., Sun, Y., Song, C., Shilling, J. E., Onasch, T. B., Herndon, S.  
582 C., Worsnop, D. R., Fast, J. D., Zaveri, R. A., Berg, L. K., Wiedensohler, A., Flowers, B. A., Dubey, M. K., and  
583 Subramanian, R.: Characterization of submicron particles influenced by mixed biogenic and anthropogenic  
584 emissions using high-resolution aerosol mass spectrometry: results from CARES, *Atmos. Chem. Phys.*, 12, 8131-  
585 8156, 2012.
- 586 Stohl, A., Trainer, M., Ryerson, T. B., Holloway, J. S., and Parrish, D. D.: Export of NO<sub>y</sub> from the North American  
587 boundary layer during 1996 and 1997 North Atlantic Regional Experiments, *J. Geophys. Res. Atmos.*, 107, 4131-  
588 4139, 2002.
- 589 Sun, Y., Zhang, Q., Macdonald, A. M., Hayden, K., Li, S. M., Liggio, J., Liu, P. S. K., Anlauf, K. G., Leaitch, W.  
590 R., Steffen, A., Cubison, M., Worsnop, D. R., van Donkelaar, A., and Martin, R. V.: Size-resolved aerosol chemistry  
591 on Whistler Mountain, Canada with a high-resolution aerosol mass spectrometer during INTEX-B, *Atmos. Chem.*  
592 *Phys.*, 9, 3095-3111, 2009.
- 593 Sun, Y. L., Zhang, Q., Schwab, J. J., Yang, T., Ng, N. L., and Demerjian, K. L.: Factor analysis of combined organic  
594 and inorganic aerosol mass spectra from high resolution aerosol mass spectrometer measurements, *Atmos. Chem.*  
595 *Phys.*, 12, 8537-8551, 2012.
- 596 Takahama, S., Schwartz, R. E., Russell, L. M., Macdonald, A. M., Sharma, S., and Leaitch, W. R.: Organic  
597 functional groups in aerosol particles from burning and non-burning forest emissions at a high-elevation mountain  
598 site, *Atmos. Chem. Phys.*, 11, 6367-6386, 2011.
- 599 Taylor, N. F., Collins, D. R., Lowenthal, D. H., McCubbin, I. B., Hallar, A. G., Samburova, V., Zielinska, B.,  
600 Kumar, N., and Mazzoleni, L. R.: Hygroscopic growth of water soluble organic carbon isolated from atmospheric  
601 aerosol collected at US national parks and Storm Peak Laboratory, *Atmos. Chem. Phys.*, 17, 2555-2571, 2017.
- 602 Timonen, H., Jaffe, D. A., Wigder, N., Hee, J., Gao, H., Pitzman, L., and Cary, R. A.: Sources of carbonaceous  
603 aerosol in the free troposphere, *Atmos. Environ.*, 92, 146-153, 2014.
- 604 Timonen, H., Wigder, N., and Jaffe, D.: Influence of background particulate matter (PM) on urban air quality in the  
605 Pacific Northwest, *J. Environ. Manage.*, 129, 333-340, 2013.
- 606 Tröstl, J., Herrmann, E., Frege, C., Bianchi, F., Molteni, U., Bukowiecki, N., Hoyle, C. R., Steinbacher, M.,  
607 Weingartner, E., Dommen, J., Gysel, M., and Baltensperger, U.: Contribution of new particle formation to the total  
608 aerosol concentration at the high-altitude site Jungfraujoch (3580 m asl, Switzerland), *J. Geophys. Res. Atmos.*,  
609 121, 11,692-611,711, 2016.



- 610 Tunved, P., Ström, J., and Krejci, R.: Arctic aerosol life cycle: linking aerosol size distributions observed between  
611 2000 and 2010 with air mass transport and precipitation at Zeppelin station, Ny-Ålesund, Svalbard, Atmos. Chem.  
612 Phys., 13, 3643-3660, 2013.
- 613 Ulbrich, I. M., Canagaratna, M. R., Zhang, Q., Worsnop, D. R., and Jimenez, J. L.: Interpretation of organic  
614 components from Positive Matrix Factorization of aerosol mass spectrometric data, Atmos. Chem. Phys., 9, 2891-  
615 2918, 2009.
- 616 Van Dingenen, R., Putaud, J. P., Martins-Dos Santos, S., and Raes, F.: Physical aerosol properties and their relation  
617 to air mass origin at Monte Cimone (Italy) during the first MINATROC campaign, Atmos. Chem. Phys., 5, 2203-  
618 2226, 2005.
- 619 Wang, J., Krejci, R., Giangrande, S., Kuang, C., Barbosa, H. M., Brito, J., Carbone, S., Chi, X., Comstock, J., Ditas,  
620 F., Lavric, J., Manninen, H. E., Mei, F., Moran-Zuloaga, D., Pohlker, C., Pohlker, M. L., Saturno, J., Schmid, B.,  
621 Souza, R. A., Springston, S. R., Tomlinson, J. M., Toto, T., Walter, D., Wimmer, D., Smith, J. N., Kulmala, M.,  
622 Machado, L. A., Artaxo, P., Andreae, M. O., Petaja, T., and Martin, S. T.: Amazon boundary layer aerosol  
623 concentration sustained by vertical transport during rainfall, Nature, 539, 416-419, 2016.
- 624 Watts, S. F.: The mass budgets of carbonyl sulfide, dimethyl sulfide, carbon disulfide and hydrogen sulfide, Atmos.  
625 Environ., 34, 761-779, 2000.
- 626 Weiss-Penzias, P., Jaffe, D. A., Swartzendruber, P., Dennison, J. B., Chand, D., Hafner, W., and Prestbo, E.:  
627 Observations of Asian air pollution in the free troposphere at Mount Bachelor Observatory during the spring of  
628 2004, J. Geophys. Res. Atmos., 111, D10304, 2006.
- 629 Worton, D. R., Goldstein, A. H., Farmer, D. K., Docherty, K. S., Jimenez, J. L., Gilman, J. B., Kuster, W. C., de  
630 Gouw, J., Williams, B. J., Kreisberg, N. M., Hering, S. V., Bench, G., McKay, M., Kristensen, K., Glasius, M.,  
631 Surratt, J. D., and Seinfeld, J. H.: Origins and composition of fine atmospheric carbonaceous aerosol in the Sierra  
632 Nevada Mountains, California, Atmos. Chem. Phys., 11, 10219-10241, 2011.
- 633 Xu, J., Zhang, Q., Shi, J., Ge, X., Xie, C., Wang, J., Kang, S., Zhang, R., and Wang, Y.: Chemical characteristics of  
634 submicron particles at the central Tibetan Plateau: insights from aerosol mass spectrometry, Atmos. Chem. Phys.,  
635 18, 427-443, 2018.
- 636 Young, D. E., Kim, H., Parworth, C., Zhou, S., Zhang, X., Cappa, C. D., Seco, R., Kim, S., and Zhang, Q.:  
637 Influences of emission sources and meteorology on aerosol chemistry in a polluted urban environment: results from  
638 DISCOVER-AQ California, Atmos. Chem. Phys., 16, 5427-5451, 2016.
- 639 Zhang, L. and Jaffe, D. A.: Trends and sources of ozone and sub-micron aerosols at the Mt. Bachelor Observatory  
640 (MBO) during 2004–2015, Atmos. Environ., 165, 143-154, 2017.
- 641 Zhang, Q., Jimenez, J. L., Canagaratna, M. R., Allan, J. D., Coe, H., Ulbrich, I., Alfarra, M. R., Takami, A.,  
642 Middlebrook, A. M., Sun, Y. L., Dzepina, K., Dunlea, E., Docherty, K., DeCarlo, P. F., Salcedo, D., Onasch, T.,  
643 Jayne, J. T., Miyoshi, T., Shimojo, A., Hatakeyama, S., Takegawa, N., Kondo, Y., Schneider, J., Drewnick, F.,  
644 Borrmann, S., Weimer, S., Demerjian, K., Williams, P., Bower, K., Bahreini, R., Cottrell, L., Griffin, R. J.,  
645 Rautiainen, J., Sun, J. Y., Zhang, Y. M., and Worsnop, D. R.: Ubiquity and dominance of oxygenated species in  
646 organic aerosols in anthropogenically-influenced Northern Hemisphere midlatitudes, Geophys Res Lett, 34, 6, 2007.

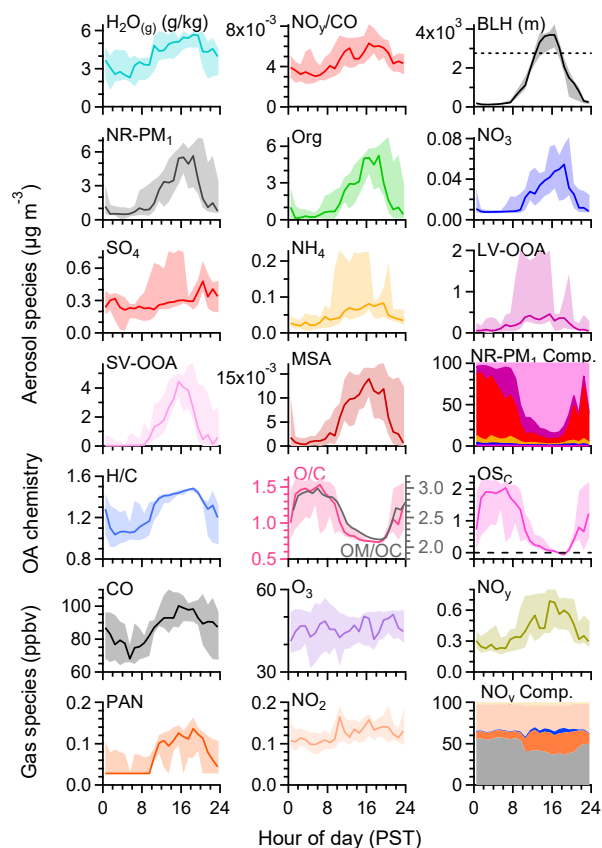


- 647 Zhang, Q., Jimenez, J. L., Canagaratna, M. R., Ulbrich, I. M., Ng, N. L., Worsnop, D. R., and Sun, Y. L.:  
648 Understanding atmospheric organic aerosols via factor analysis of aerosol mass spectrometry: a review, *Anal*  
649 *Bioanal Chem*, 401, 3045-3067, 2011.
- 650 Zhang, Q., S. Zhou, S. Collier, D. Jaffe, T. Onasch, J. Shilling, L. Kleinman, and A. Sedlacek: Understanding  
651 Composition, Formation, and Aging of Organic Aerosols in Wildfire Emissions via Combined Mountain Top and  
652 Airborne Measurements, . In: *Multiphase Environmental Chemistry in the Atmosphere*, American Chemical Society  
653 (ACS) Books, 2018.
- 654 Zhou, S., Collier, S., Jaffe, D. A., Briggs, N. L., Hee, J., Sedlacek Iii, A. J., Kleinman, L., Onasch, T. B., and Zhang,  
655 Q.: Regional influence of wildfires on aerosol chemistry in the western US and insights into atmospheric aging of  
656 biomass burning organic aerosol, *Atmos. Chem. Phys.*, 17, 2477-2493, 2017.
- 657 Zhou, S., Collier, S., Xu, J., Mei, F., Wang, J., Lee, Y.-N., Sedlacek, A. J., Springston, S. R., Sun, Y., and Zhang,  
658 Q.: Influences of upwind emission sources and atmospheric processing on aerosol chemistry and properties at a rural  
659 location in the Northeastern U.S, *J. Geophys. Res. Atmos.*, 121, 6049-6065, 2016.
- 660 Zhu, Q., He, L. Y., Huang, X. F., Cao, L. M., Gong, Z. H., Wang, C., Zhuang, X., and Hu, M.: Atmospheric aerosol  
661 compositions and sources at two national background sites in northern and southern China, *Atmos. Chem. Phys.*, 16,  
662 10283-10297, 2016.
- 663 Zorn, S. R., Drewnick, F., Schott, M., Hoffmann, T., and Borrmann, S.: Characterization of the South Atlantic  
664 marine boundary layer aerosol using an aerodyne aerosol mass spectrometer, *Atmos. Chem. Phys.*, 8, 4711-4728,  
665 2008.
- 666



667

668 **Fig. 1.** Observations during two clean periods in summer 2013. Time series of (a) wind direction (WD) colored  
669 by wind speed (WS), (b) mixing ratios of CO and water vapor ( $\text{H}_2\text{O}_{(\text{g})}$ ) (c - e) mass concentrations of NR-PM<sub>1</sub> species  
670 and OA factors ( $\mu\text{g m}^{-3}$ ), and organic-equivalent mass concentration of MSA ( $\text{ng m}^{-3}$ ) at ambient conditions,  
671 submicron aerosol light scattering at 550 nm ( $\sigma_{550\text{nm}}$ ), (f) NR-PM<sub>1</sub> composition, and (g) OA composition.



672

673

674

675

676

677

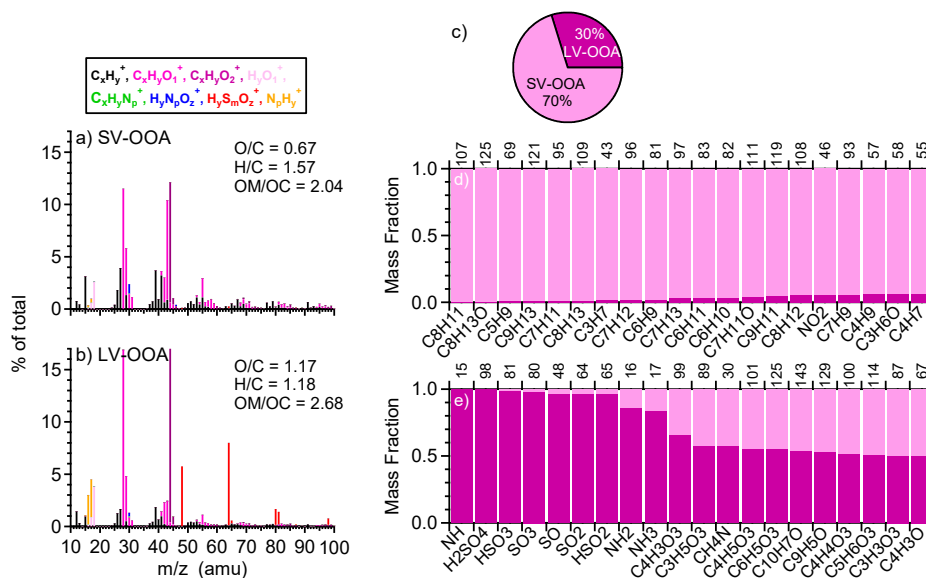
678

679

680

681

**Fig. 2.** Median diurnal cycles of water vapor ( $\text{H}_2\text{O}_{(\text{g})}$ ),  $\text{NO}_y/\text{CO}$  ratio (ppb/ppb), estimated boundary layer height (BLH), mass concentrations of NR- $\text{PM}_{10}$  species, OA chemistry, and mixing ratios of gas species during the clean periods shown in Fig. 1 at MBO. MSA is in organic equivalent mass concentration. Oxidation state of carbon ( $\text{OS}_\text{C}$ ) =  $2 \text{O/C} - \text{H/C}$ . The shaded areas indicate the 75th and 25th percentiles. The diurnal cycle of NR- $\text{PM}_{10}$  composition displays the percent mass contributions, from top to bottom, of SV-OOA in light pink, LV-OOA in dark purple, sulfate in red, ammonium in orange, nitrate in blue, and chloride in purple. The diurnal cycle of  $\text{NO}_y$  composition displays the percent mixing ratio contributions, from top to bottom, of NO in yellow,  $\text{NO}_2$  in light orange, nitrate in blue, PAN in dark orange, and  $\text{NO}_z$  ( $= \text{NO}_y - \text{NO} - \text{NO}_2 - \text{nitrate} - \text{PAN}$ ) in grey. Dashed line in BLH indicates the altitude of MBO (2763 m).



682

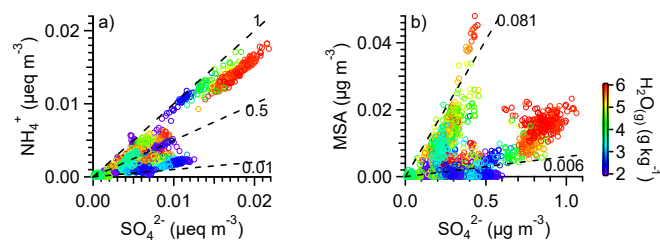
683

684 **Fig. 3.** High resolution mass spectrum of (a) SV-OOA and (b) LV-OOA colored by eight ion families. The

685 elemental ratios of OA determined using the IA method are shown in the legends. (c) Average OA composition. (d-e)

686 Ion signal distribution between SV-OOA and LV-OOA. Top 20 ions with greater fraction in SV-OOA in (d) and those

with greater fraction in LV-OOA in (e). The nominal masses of the ions are shown on the top axes of (d) and (e).



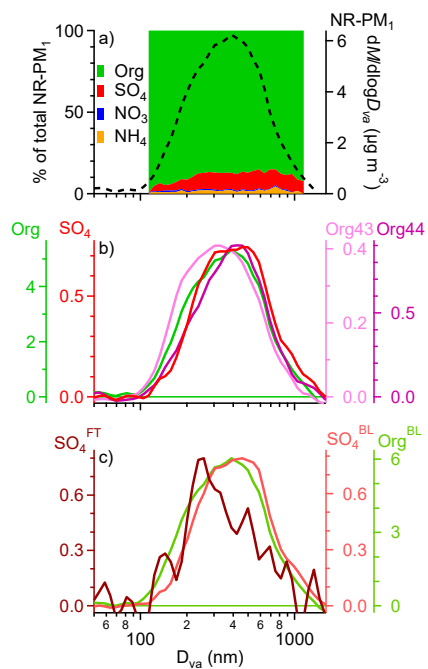
687

688

689

690

**Fig. 4.** (a) Ammonium molar equivalent concentration ( $[\text{NH}_4^+]/18$ ) vs. sulfate molar equivalent concentration ( $[\text{SO}_4^{2-}]/48$ ) and (b) MSA mass concentration vs. sulfate mass concentration colored by water vapor mixing ratio. Dashed lines with different slopes are added for reference.



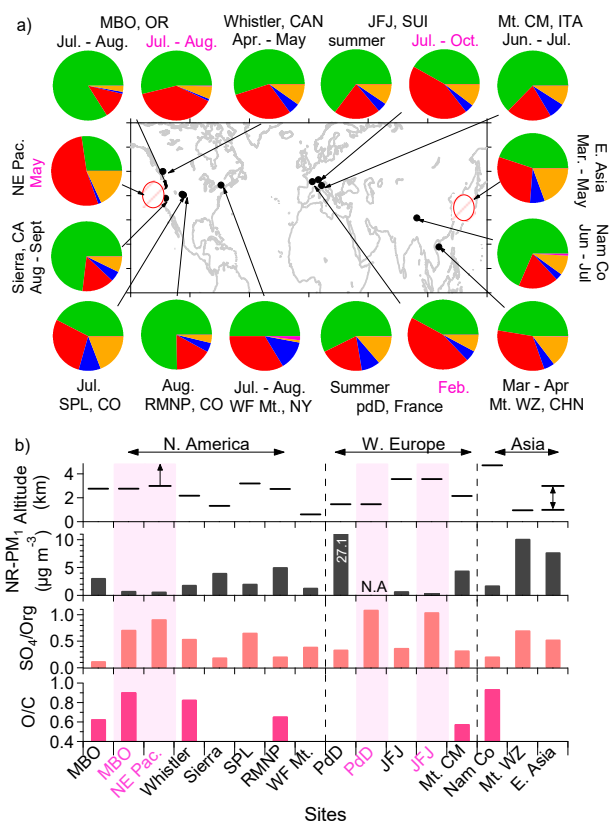
691

692

693

694

**Fig. 5.** (a) Size-resolved aerosol composition on the left axis, average size distributions of total NR-PM<sub>1</sub> mass on the right. (b) Average mass size distributions of organics, sulfate, Org43, and Org44 during the clean periods. (c) Average mass size distributions of FT sulfate and BL influenced sulfate and organics.



695

696

697

698

699

700

701

702

**Fig. 6.** (a) Location of selected high-altitude mountain sites and aircraft measurements of regional background aerosols in the world and the chemical composition of NR-PM<sub>1</sub> (details listed in Table S1 in the Supplement). Pie charts show the average chemical composition: organics (green), sulfate (red), nitrate (blue), ammonium (orange), and chloride (purple) of NR-PM<sub>1</sub>. (b) Sampling altitude, average NR-PM<sub>1</sub> mass concentration, sulfate-to-organic mass ratio (SO<sub>4</sub>/Org), and average O/C ratio of OA determined from the Ambient-Aiken method for each site. Colors of sampling period labels for pie charts in (a) and bottom axis labels for sites in (b) indicate air mass type: mixed BL/FT air (black) or FT air only (pink). Shaded pink bars in (b) indicate FT air.